Corresponding author: V.V. Atuchin
Institute of Semiconductor Physics, Novosibirsk 630090, Russia
Phone: +7 (383) 3308889
E-mail: atuchin@isp.nsc.ru

Exploration of structural, vibrational and spectroscopic properties of self-activated orthorhombic double molybdate $RbEu(MoO_4)_2$ with isolated MoO_4 units

Victor V. Atuchin[1,2,3,4,*], Aleksandr S. Aleksandrovsky[5,6], Bair G. Bazarov[7,8], Jibzema G. Bazarova[7], Olga D. Chimitova[7], Yuriy G. Denisenko[9], Tatyana A. Gavrilova[10], Alexander S. Krylov[11], Eugene A. Maximovskiy[12], Maxim S. Molokeev[13,14,15], Aleksandr S. Oreshonkov[11,15], Alexey M. Pugachev[16], Nikolay V. Surovtsev[16]

[1]Laboratory of Optical Materials and Structures, Institute of Semiconductor Physics, SB RAS, Novosibirsk 630090, Russia

[2]Functional Electronics Laboratory, Tomsk State University, Tomsk 634050, Russia

[3]Laboratory of Single Crystal Growth, South Ural State University, Chelyabinsk 454080, Russia

[4]Research and Development Department, Kemerovo State University, Kemerovo 650000, Russia

[5]Laboratory of Coherent Optics, Kirensky Institute of Physics Federal Research Center KSC SB RAS, Krasnoyarsk 660036, Russia

[6]Department of Photonics and Laser Technologies, Siberian Federal University, Krasnoyarsk 660079, Russia

[7]Laboratory of Oxide Systems, Baikal Institute of Nature Management, SB RAS, Ulan-Ude 670047, Russia

[8]Buryat State University, Ulan-Ude 670000, Russia

[9]Department of General and Special Chemistry, Industrial University of Tyumen, Tyumen 625000, Russia

[10]Laboratory of Nanodiagnostics and Nanolithography, Institute of Semiconductor Physics, SB RAS, Novosibirsk 630090, Russia

[11]Laboratory of Molecular Spectroscopy, Kirensky Institute of Physics Federal Research Center KSC SB RAS, Krasnoyarsk 660036, Russia

[12]Laboratory of Functional Films and Coatings, Institute of Inorganic Chemistry, SB RAS, Novosibirsk 630090, Russia

[13]Laboratory of Crystal Physics, Kirensky Institute of Physics Federal Research Center KSC SB RAS, Krasnoyarsk 660036, Russia

[14]Department of Physics, Far Eastern State Transport University, Khabarovsk 680021, Russia

[15]Siberian Federal University, Krasnoyarsk 660079, Russia

[16]Laboratory of Condensed Matter Spectroscopy, Institute of Automation and Electrometry, SB RAS, Novosibirsk 630090, Russia

Abstract

$RbEu(MoO_4)_2$ is synthesized by the two-step solid state reaction method. The crystal structure of $RbEu(MoO_4)_2$ is defined by Rietveld analysis in space group *Pbcn* with cell parameters a=5.13502(5), b=18.8581(2) and c=8.12849(7) Å, V=787.13(1) $Å^3$, Z=4 (R_B=0.86%). This molybdate possesses its phase transition at 817 K and melts at 1250K. The Raman spectra were measured with the excitation at λ=1064 and 514.5nm. The photoluminescence spectrum is evaluated under the excitation at 514.5nm. The absolute domination of hypersensitive $^5D_0 \rightarrow {}^7F_2$ transition is observed. The ultranarrow $^5D_0 \rightarrow {}^7F_0$ transition in $RbEu(MoO_4)_2$ is positioned at 580.2nm being 0.2nm blue shifted, with respect to that in $Eu_2(MoO_4)_3$.

Keywords: rubidium europium molybdate; solid state reaction; Rietveld refinement; DSC; Raman luminescence

1. Introduction

In modern photonics, the crystals containing europium ions are of particular interest because of the efficient red emission provided by Eu^{3+} ions under the short-wavelength excitation and this property is extremely needed for the WLED devices and other optical systems [1-5]. By now, a lot of different Eu^{3+}-doped phosphors with a complex structure have been proposed and their spectroscopic properties have been evaluated [6-12]. However, in the solid solutions, the Eu^{3+} doping level is commonly low to avoid the concentration-quenching effects and, respectively, the crystallographic positions of Eu^{3+} ions may be not evident. In this case, it is difficult to exhibit in detail the correlations between the photoluminescence parameters and crystallographic environment of Eu^{3+} ions. To solve the problem, the europium compounds can be considered because, in this case, the Eu^{3+} ion positions can be precisely determined by the methods of crystal structure analysis [13-20].

In the present study, new binary molybdate $RbEu(MoO_4)_2$ is considered for the first time. Available information on the existence and structural properties of molybdates with general composition $RbLn(MoO_4)_2$ is very limited [21]. Recently, $RbNd(MoO_4)_2$ and $RbSm(MoO_4)_2$ molybdates have been synthesized, their structures have been defined in space group *Pbcn* and electronic structures have been calculated [20-25]. The set of heavier Ln elements, where the formation of orthorhombic structure is possible, remains unclear because, to our best knowledge, only $RbYb(MoO_4)_2$ and $RbLu(MoO_4)_2$ were considered earlier and monoclinic, and trigonal symmetries, respectively, were reported for the compounds [26,27]. Thus, the present work is aimed at the evaluation of structural and spectroscopic characteristics of $RbEu(MoO_4)_2$ and comparative observation of the properties within the set of $RbLn(MoO_4)_2$ (Ln = Nd, Sm, Eu).

2. Experimental

The commercial MoO_3 (99.99%, Red Chemist, Ltd., Russia), Rb_2CO_3 (99.9%, Aldrich) and Eu_2O_3 (99.99%, Red Chemist, Ltd., Russia) were taken as the starting materials. The crystalline molybdate samples were prepared in ceramic crucibles using the solid state reaction method. Initially, Rb_2MoO_4 and $Eu_2(MoO_4)_3$ were obtained. The heat treatment of stoichiometric mixtures of the initial materials was started at T = 450 °C and followed by a step-wise temperature increase up to T = 600 °C (Rb_2MoO_4) and 1000 °C ($Eu_2(MoO_4)_3$). Then, to prepare the starting charge for the synthesis of $RbEu(MoO_4)_2$, the Rb_2MoO_4 and $Eu_2(MoO_4)_3$ molybdates were ground and mixed in stoichiometric composition Rb_2MoO_4:$Eu_2(MoO_4)_3$ = 1:1. After that, the mixture was heated to 490°C and kept for about 70 h and, then, it was fired at T = 600°C by 150 h to yield $RbEu(MoO_4)_2$. The temperature was controlled at a precision of ±2°C up to 1200°C with an OMRON controller. After the heat treatment, the sample was slowly cooled to room temperature together with the furnace at an estimated cooling rate of ~12°C/min.

The final powder product micromorphology was observed by scanning electron microscopy (SEM) with the use of an LEO 1430 electron microscope. The chemical composition of the powder sample was measured by a scanning electron microscope Hitachi S-3400N equipped by an energy dispersive spectrometer INCA Energy 350 manufactured by Oxford Instruments. The composition measurements were averaged over the area of 100×100 μm^2, the electron beam energy was 20 keV and the beam current was 0,5 nA.

The powder X-ray diffraction data were recorded by a D8 ADVANCE Bruker AXS diffractometer (Vantec-1 detector) at room temperature using the CuK_α radiation and scanning over the range of 2θ = 8-140°. The variable counting time (VCT) and step size (VSS) scheme were used to collect the diffraction data. The measurement time was systematically increased towards higher 2θ angles, leading to a drastically improved data quality [28], and this algorithm was proved in several contributions [29-31]. To collect the X-ray data using a VCT scheme, four ranges were generated on the diffraction pattern: 5°–38.5° (exposure per point: 1 s; step: 0.016°), 38.5°–60.5°

(exposure per point: 3 s; step: 0.024°), 60.5°–97.5° (exposure per point: 5 s; step: 0.032°) and 97.5°–140° (exposure per point: 8 s; step: 0.040°). The total experimental time was equal to 6 h. Rietveld refinement was performed using TOPAS 4.2 [32].

The differential scanning calorimetry (DSC) measurements were performed by means of a simultaneous thermal analyzer NETZSCH STA 449 F3 Jupiter, in the temperature range from 400 to 1423 K at the heating rate of 10 K/min. The $RbEu(MoO_4)_2$ powder was placed into the Pt crucible and heated up and cooled down in the Ar atmosphere.

The unpolarized Raman study of the powder sample was carried out in a back-scattering geometry. To avoid the possible confusion between the Raman lines and photoluminescence lines of Eu^{3+} ions, two sets of experiments were carried out, with 514.5 and 1064 nm wavelengths of laser excitations. The Raman experiment with the Nd:YAG laser (1064 nm) was carried out on Raman spectrometer Bruker RFS/100 (spectral resolution 2 cm^{-1}). The laser irradiation of an argon laser (514.5 nm, Spectra-Physics Stabilite 2017) was used for the Raman experiment after passing a monochromator [33] to suppress laser plasma lines. The laser beam was focused on the sample by a lens with the focal length of 60 mm, and this lens collected the scattered light. A triple-grating spectrometer TriVista 777 was used for the Raman scattering registration in a single stage mode (single grating plus a notch filter) to collect a signal for the Raman shift from 530 to 1070 cm^{-1} and in the triple-grating mode for the Raman shift from 20 to 560 cm^{-1}. the spectral resolution was ~2.5 cm^{-1}. The wavelength calibration of the spectra was made by a comparison of a neon-discharge lamp spectrum with the tabular data.

The high-resolution luminescence spectra were recorded with the help of the triple-monochromator Horiba Jobin Yvon T64000 Raman spectrometer in the 180^o geometry and in a double subtractive mode. A liquid-nitrogen-cooled Symphony CCD detector was used for the collection of luminescence. Employing 100 μm slits and 1800 g/mm enabled achieving the spectral resolution as high as 4 cm^{-1} for luminescence measurements. The samples were placed within the focal plane of Olympus BX41 microscope with a Olympus 50^x objective lens (f = 0.8 mm

NA=0.75) that enabled a 2 μm focal spot at the sample. The excitation of luminescence spectra was performed using the 514.5 nm line from a single-mode Spectra-Physics Stabilite 2017 Ar^+ laser, the power of the excitation being limited to 5 mW at the sample.

3. Results and discussions

The final high temperature synthesis product was found to be of light-cream color that is common for Eu^{3+}-containing oxide compounds [13,17,34-36]. A typical SEM image of the powder sample is shown in Fig. 1. As seen, the synthesis resulted in the agglomerates 2-20 μm in size formed by partly coalescent individual plate-like partly-faceted grains with a diameter below 1-5 μm. The faceted micromorphology is common for molybdates when the temperature/time conditions used in the synthesis are high enough for the active oxide grain interdiffusion and possible material exchange *via* the MoO_3 vapor [17,37,38]. Typically, the presence of faceted microcrystals in the powder is a robust indicator of a high structural quality of the sample [17,25,33]. Besides, it should be pointed that the $RbEu(MoO_4)_2$ particles possess a strong charging effect during SEM measurements and this reveals their very low conductivity common for the oxides without oxygen vacancies. The chemical composition of the sample, as obtained by EDS, is shown in Table S1. The results are in a good relation to nominal composition Rb:Eu:Mo:O = 8.3:8.3:16.7:66.7.

The initial examination of the XRD pattern of the synthesized powder sample revealed that it resembles that of $RbNd(MoO_4)_2$ [20]. The final Rietveld profiles are shown in Fig. 2. There are no foreign diffraction peaks and all peaks of the XRD pattern were indexed by an orthorhombic cell (space group *Pbcn*) with parameters close to those of $RbNd(MoO_4)_2$ [20]. Therefore, the crystal structure of $RbNd(MoO_4)_2$ was taken as a starting model for Rietveld refinement. All thermal parameters of ions were refined at the isotropic approximation and individually. The refinement was stable and gave low *R*-factors (Table 1, Fig. 2). The atom coordinates and main bond lengths obtained for $RbEu(MoO_4)_2$ are summarized in Table 2S and Table 3S, respectively.

The obtained $RbEu(MoO_4)_2$ structure is illustrated in Fig. 3. The asymmetric unit cell of $RbEu(MoO_4)_2$ crystal structure contains one Rb^+, one Eu^{3+}, one Mo^{6+} and four O^{2-} ions. The Rb^+ and Eu^{3+} ions are located in special Wyckoff sites 4c with local symmetry C_2. The Rb^+ ion is coordinated by six O^{2-} ions (d(Rb–O) = 2.798 (8)–2.98 (1) Å) forming a distorted octahedron, while the Eu^{3+} ion is coordinated by eight O^{2-} ions (d(Eu–O) = 2.34(1)–2.59(1) Å) forming a square antiprism. The Mo^{6+} ion is located in general site 8*d* and it is coordinated by four O^{2-} ions forming a tetrahedron. This tetrahedron is linked with EuO_8 and RbO_6 polyhedrons by nodes and, formally, the MoO_4 group is a bridge between these two polyhedrons. In addition, EuO_8 polyhedrons are linked with each other by the edges forming the columns along the *c*-axis, RbO_6 polyhedrons are joined with each other by the nodes forming a 2D layer in the *ac* plane and EuO_8 with RbO_6 are linked by the edges forming a 3D network. The topological analysis of the net by ToposPro program [39], using simplification that Eu^{3+}, Rb^+ and Mo^{6+} are first, second and third nodes, revealed that this is a 3-nodal $(7\text{-c})_2(11\text{-c})(11\text{-c})$ net with point symbol $(3^{12}.4^{23}.5^{18}.6^2)(3^{12}.4^{24}.5^{14}.6^5)(3^6.4^{13}.5^2)_2$ which is new.

Two endothermic signals at 817 and 1250 K were detected upon the sample heating (Fig. 4a). During cooling, $RbEu(MoO_4)_2$ shows an exothermic effect confirming the crystallization temperature at 1197 K. One phase transition (PT) at 817 K (onset on heating) and at 769 K (onset on cooling) was detected thus confirmed that the phase transition in $RbEu(MoO_4)_2$ is reversible. To estimate character of the endoeffect, the temperature program was carried out in the mode 2 heating and 2 cooling cycles [40]. Changing of the temperature scanning direction for composition $RbEu(MoO_4)_2$ allows fixing the temperature hysteresis (Fig. 4b). The reversible phase transition was also confirmed by XRD, where XRD patterns before and after the phase change were different.

The Raman spectra of $RbEu(MoO_4)_2$ powder obtained with the excitations at 1064 and 514.5 nm shown in Figure 5. The appearance of luminescent lines $^5D_1$–$^7F_0$ of Eu^{3+} ions is observed at 442 and 459 cm^{-1} under the excitation at 514.5 nm, and, also, the Raman signal in the high-wavenumber range is overlapped with the luminescent band $^5D_1$–$^7F_1$ of Eu^{3+} ions, as was shown in [17]. The

group theory analysis predicts 72 Raman-active modes for the $RbEu(MoO_4)_2$ crystal in the D^{14}_{2h} structure. These modes are distributed among the irreducible representations as $17A_g+19B_{1g}+17B_{2g}+19B_{3g}$. The free tetrahedral MoO_4^{2-} ion has four normal vibration modes. All modes are Raman active (ν_1 symmetric stretching (A_1), ν_2 symmetric bending (E), ν_3 antisymmetric stretching (T_2) and ν_4 antisymmetric bending (T_2)) [41]. In the case of $RbEu(MoO_4)_2$, the site symmetry of MoO_4^{2-} ions (C_1) is lower than that of isolated molecule (T_d), and that leads to the splitting of double degenerate E and triply degenerate T_2 modes. From the correlation diagram shown in Table 2, one can conclude that four lines can appear in the region of symmetric stretching and twelve modes can appear in the region of antisymmetric stretching of the MoO_4^{2-} ion, and that explains a complex spectral shape in this wavenumber range. It is interesting to compare the Raman spectra of orthorhombic crystals $RbLn(MoO_4)_2$ (Ln = Nd, Sm, Eu), as shown in Fig. 6 [22,23]. The isomorphic replacement of rare-earth ion in the $RbLn(MoO_4)_2$ (Ln = Nd, Sm, Eu) family leads to differences in the lattice parameters and bond length values of MoO_4^{2-} ions, and that, in turn, leads to the differences in wavenumber values in the region of stretching (Fig. 6a) and bending vibrations (Fig. 6b).

The overview of $RbEu(MoO_4)_2$ photoluminescence spectrum under the excitation at 514.5 nm is given in Fig. 7. The longer wavelength part of the spectrum is multiplied by 3000 to reveal the weakest transitions. More detailed spectra of each band are presented in Supplementary materials (Fig. S1). An interesting feature of Eu ion luminescence spectra in orthorhombic $RbEu(MoO_4)_2$ is the absolute domination of hypersensitive $^5D_0 \rightarrow {}^7F_2$ transition, for instance, in comparison with the tetragonal $Eu:NaGd(WO_4)_2$ crystal [42]. A similar feature was earlier observed for monoclinic $Eu_2(MoO_4)_3$. Additionally, the domination of a single component corresponding to a transition between crystal field split sublevels within the $^5D_0 \rightarrow {}^7F_2$, $^5D_0 \rightarrow {}^7F_3$ and $^5D_0 \rightarrow {}^7F_4$ bands was observed. These features, generally speaking, are favorable for obtaining the laser generation at the $^5D_0 \rightarrow {}^7F_2$ transition that has not been obtained yet at room temperature, since single dominated line

in the luminescence must unavoidably result in the increase of stimulated emission cross section within a narrow spectral range of this line.

To evaluate the relative efficiency of Eu^{3+} luminescence in $RbEu(MoO_4)_2$, we compared the luminescence intensities of equivalent samples of $RbEu(MoO_4)_2$ and monoclinic $Eu_2(MoO_4)_3$ under identical spectrometer settings. The luminescence in $RbEu(MoO_4)_2$ peaks at 613.9 nm with the intensity of 2.25 times smaller than the corresponding peak in $Eu_2(MoO_4)_3$ (at 615.6 nm). In view of the high Eu concentration in both crystals, this intensity ratio mainly characterizes the competition between the radiative probability and the influence of concentration quenching. However, the difference in the Eu content must be accounted for. From the crystal structure data, the Eu content per cm^3 in $RbEu(MoO_4)_2$ is 1.67 times smaller than that in $Eu_2(MoO_4)_3$. Due to the similarity of higher-energy vibrational spectra of both crystals, the influence of concentration quenching can be roughly estimated to be the same in both crystals. Taking all these obstacles into considerations, we can deduce that the effect of the absence of central inversion symmetry that contributes to the rise of oscillator strength at the hypersensitive transition is approximately the same both in the crystal under study and in the reference crystal.

The ultranarrow $^5D_0 \rightarrow {}^7F_0$ transition in $RbEu(MoO_4)_2$ is positioned at 580.2 nm being 0.2 nm blue shifted, with respect to the reference crystal. Its width is approximately the same as in the europium molybdate, while the intensity is 16 times smaller. Since both hypersensitive and ultranarrow transitions start from the same luminescing level, the difference in the relative intensity of these transitions in two crystals must be ascribed exclusively to the local symmetry of Eu^{3+} ions. The latter in monoclinic europium molybdate is C_1, while it is C_2 in $RbEu(MoO_4)_2$. Both symmetries are favorable for breaking the prohibition of the transition between J=0 states. Therefore, we must conclude that mirror symmetry violation effect of the local environment of the Eu^{3+} ion in $RbEu(MoO_4)_2$ is much smaller than that in $Eu_2(MoO_4)_3$.

4. Conclusions

In the $KY(MoO_4)_2$ molybdate family, a new orthorhombic Rb-containing molybdate $RbEu(MoO_4)_2$ is discovered, and this further extends the nomenclature of double molybdate crystals available in this family. As it is clear, this molybdate family covers a wide range of alkaline and rare earth elements, including those appropriate for laser and photonic applications, covering the creation of new phosphors. Thus, wider design and deep investigation of the compounds related to the $ALn(MoO_4)_2$ (*A* = Tl, alkaline metals; *Ln* = Y, rare earth metals) crystal family is topical, including a search for new compounds and solid solutions, the development of crystal growth methods, observation of electronic and luminescence characteristics. This opens a door for the estimation of this molybdate family potential for practical applications. The luminescence properties of Eu^{3+} ions indicate that the Eu-activated crystals of the $ALn(MoO_4)_2$ family (*Ln* = Gd, La and probably Y and Lu) can be designed and they could be good candidates for self-doubling Eu-lasing media.

Supporting Information

Structural cif file, checkcif file, EDS data, atom coordinates, bond lengths, luminescence spectra.

Author information

The authors declare no competing financial interest.

Acknowledgements

The reported study was funded by RFBR according to research projects 16-52-48010, 17-52-53031 and 18-03-00557. Besides. this study was supported by the Ministry of Science and Higher Education of the Russian Federation (project 0339-2016-0007). The work was supported by Act 211 Government of the Russian Federation, contract № 02.A03.21.0011. Additionally the work was partially supported by the Ministry of Education and Science of the Russian Federation (4.1346.2017/4.6).

References

1. Chun Che Lin and Ru-Shi Liu, Advances in phosphors for light-emitting diodes, J. Phys. Chem. Lett. 2 (2011) 1268-1277.
2. P.A. Tanner, Some misconceptions concerning the electronic spectra of tri-positive europium and cerium, Chem. Soc. Rev. 42 (2013) 5090-5101.
3. Mengmeng Shang, Chunxia Li, Jun Lin, How to produce white light in a single-phase host, Chem. Soc. Rev. 43 (5) (2014) 1372-1386.
4. Kai Li, Mengmeng Shang, Hongzhou Lian, Jun Lin, Recent development in phosphors with different emitting colors viua energy transfer, J. Mater. Chem. C 4 (2016) 5507-5530.
5. Zhiguo Xia, Quankin Liu, Progress in discovery and structural design of color conversion phosphors for LEDs, Prog. Mater. Sci. 54 (2016) 59-117.
6. Zhiguo Xia, Shuai Jin, Jiayue Sun, Halyan Du, Peng Du, Libing Liao, Facile morphology-controlled synthesis and luminescence properties of $BaMoO_4:Eu^{3+}$ microparticles and micro-rods obtained by a molten-salt reaction route, J. Nanosci. Nanotech. 11 (2011) 9612-9620.
7. P.S. Dutta, A. Khanna, Eu^{3+} activated molybdate and tungstate based red phosphors with charge transfer band in blue region, ECS J. Solid State Sci. Technol. 2 (2) (2013) R3153-R3167.
8. Hekai Zhu, Zhiguo Xia, Haikun Liu, Ruiyu Mi, Zhuang Hui, Luminescence properties and energy transfer of Bi^{3+}/Eu^{3+}-codoped $Ca_{10}(PO_4)_6F_2$ phosphors, Mater. Res. Bull. 48 (2013) 3513-3517.
9. I.E. Kolesnikov, D.V. Tolstikova, A.V. Manshina, M.D. Mikhailov, Eu^{3+} concentration effect on luminescence properties of $YAG:Eu^{3+}$ nanoparticles, Opt. Mater. 37 (2014) 306-310.
10. Pinglu Shi, Zhiguo Xia, M.S. Molokeev, V.V. Atuchin, Crystal chemistry and luminescence properties of red-emitting $CsGd_{1-x}Eu_x(MoO_4)_2$ solid-solution phosphors, Dalton Trans. 43 (2014) 9669-9676.

11. Xiaochun Wu, Ping Xiao, Yongquan Guo, Qiaoji Zheng, Dunmin Lin, Structure, ferroelectric and photoluminescence properties of Eu-doped $CaBi_4Ti_4O_{15}$ multifunctional ceramics, J. Elect. Mater. 44 (2015) 3696-3703.
12. Fangrui Cheng, Zhiguo Xia, Maxim S. Molokeev, Xiping Jing, Effects of composition modulation on the luminescence proeprties of Eu^{3+} doped $Li_{1-x}Ag_xLu(MoO_4)_2$ solid-solution phosphors, Dalton Trans. 44 (41) (2015) 18078-18089.
13. A.S. Aleksandrovsky, V.G. Arkhipkin, L.N. Bezmaternykh, A.I. Gudim, A.S. Krylov, F. Vagizov, Origin of color centers in the flux-grown europium gallium garnet, J. Appl. Phys. 103 (8) (2008) 083102.
14. S. Zouari, R. Ballou, A. Cheikh-Rouhou, P. Strobel, Synthesis and structure of new pyrochlore-type oxides Ln_2ScNbO_7 (Ln = Pr, Nd, Eu, Gd, Dy), Mater. Lett. 62 (21-22) (2008) 3767-3769.
15. Feng Liu, J.D. Budai, Xufan Li, J.Z. Tischler, J.Y. Howe, Chengjun Sun, R.S. Meltzer, Zhengwei Pan, New ternary europium aluminate luminescent nanoribbons for advanced photonics, Adv. Func. Mater. 23 (2013) 1998-2006.
16. Tao Wu, Yunfei Liu, Yinong Lu, Ling Wei, Hong Gao, Hu Chen, Morphology-controlled synthesis, characterization, and luminescence properties of $KEu(MoO_4)_2$ microcrystals, CrystEngComm 15 (2013) 2761-2768.
17. V.V. Atuchin, A.S. Aleksandrovsky, O.D. Chimitova, T.A. Gavrilova, A.S. Krylov, M.S. Molokeev, A.S. Oreshonkov, B.G. Bazarov, J.G. Bazarova, Synthesis and spectroscopic properties of monoclinic α-$Eu_2(MoO_4)_3$, J. Phys. Chem. C 118 (2014) 15404-15411.
18. Haipeng Ji, Zhaohui Huang, Zhiguo Xia, M.S. Molokeev, Xingxing Jiang, Zheshuai Lin, V.V. Atuchin, Comparative investigations of the crystal structure and photoluminescence property of eulytite-type $Ba_3Eu(PO_4)_3$ and $Sr_3Eu(PO_4)_3$, Dalton Trans. 44 (2015) 7679-7686.
19. Yu.G. Denisenko, A.S. Aleksandrovsky, V.V. Atuchin, A.S. Krylov, M.S. Molokeev, A.S. Oreshonkov, N.P. Shestakov, O.V. Andreev, Exploration of structural, thermal and

spectroscopic properties of self-activated sulfate $Eu_2(SO_4)_3$ with isolated SO_4 groups, J. Indust. Eng. Chem. (2018), DOI: 10.1016/j.jiec.2018.07.034.

20. Yuriy G. Denisenko, Victor V. Atuchin, Maxim S. Molokeev, Aleksandr S. Aleksandrovsky, Alexander S. Krylov, Aleksandr S. Oreshonkov, Svetlana S. Volkova, Oleg V. Andreev, Structure, thermal stability, and spectroscopic properties of triclinic double sulfate $AgEu(SO_4)_2$ with isolated SO_4 groups, Inorg. Chem. (2018), DOI: 10.1021/acs.inorgchem.8b01837.
21. O.D. Chimitova, V.V. Atuchin, B.G. Bazarov, M.S. Molokeev, Z.G. Bazarova, The formation and structural parameters of new double molybdates $RbLn(MoO_4)_2$ (Ln = Pr, Nd, Sm, Eu), Proc. SPIE 8771 (2013) 87711A.
22. V.V. Atuchin, O.D. Chimitova, T.A. Gavrilova, M.S. Molokeev, Sung-Jin Kim, N.V. Surovtsev, B.G. Bazarov, Synthesis, structural and vibrational properties of microcrystalline $RbNd(MoO_4)_2$, J. Cryst. Growth 318 (2011) 683-686.
23. V.V. Atuchin, O.D. Chimitova, S.V. Adichtchev, J.G. Bazarov, T.A. Gavrilova, M.S. Molokeev, N.V. Surovtsev, Zh.G. Bazarova, Synthesis, structural and vibrational properties of microcrystalline β-$RbSm(MoO_4)_2$, Mater. Lett. 106 (2013) 26-29.
24. A.H. Reshak, Microcrystalline β-$RbNd(MoO_4)_2$: spin polarized DFT+U, RSC. Adv. 5 (2015) 44960-44968.
25. V.V. Atuchin, A.S. Aleksandrovsky, O.D. Chimitova, Cheng-Peng Diao, T.A. Gavrilova, V.G. Kesler, M.S. Molokeev, A.S. Krylov, B.G. Bazarov, J.G. Bazarova, Zheshuai Lin, Electronic structure of β-$RbSm(MoO_4)_2$ and chemical bonding in molybdates, Dalton Trans. 44 (2015) 1805-1815.
26. V.I. Spitsyn, V.K. Trunov, New data about double tungstates and molybdates with composition $MeLn(MoO_4)_2$, Dokl. Ak. Nauk USSR 185 (4) (1969) 854-855.
27. R.F. Klevtsova, P.V. Klevtsov, Polymorphysm of $RbPr(MoO_4)_2$ molybdate, Krystallographya 15 (3) (1970) 466-470.

28. I.C. Madsen, R.J. Hill, Collection and analysis of powder diffraction data with near-constant counting statistics, J. Appl. Crystallog. 27 (3) (1994) 385-392.
29. M.S. Molokeev, E.V. Bogdanov, S.V. Misyul, A. Tressaud, I.N. Flerov, Crystal structure and phase transition mechanisms in $CsFe_2F_6$, J. Solid State Chem. 200 (2013) 157-164.
30. N.N. Golovnev, M.S. Molokeev, S.N. Vereshchagin, V.V. Atuchin, M.Y. Sidorenko, M.S. Dmitrushkov, Crystal structure and properties of the precursor $[Ni(H_2O)_6](HTBA)_2{\cdot}2H_2O$ and the complexes $M(HTBA)_2(H_2O)_2$ (M = Ni, Co, Fe), Polyhedron 70 (2014) 71-76.
31. V.V. Atuchin, N.F. Beisel, E.N. Galashov, E.M. Mandrik, M.S. Molokeev, A.P. Yelisseyev, A.A. Yusuf, Zhiguo Xia, Pressure-stimulated synthesis and luminescence properties of microcrystalline $(Lu,Y)_3Al_5O_{12}:Ce^{3+}$ garnet phosphors, ACS Appl. Mater. Interfaces 7 (2015) 26235-26243.
32. Bruker AXS TOPAS V4: General profile and structure analysis software for powder diffraction data. – User's Manual. Bruker AXS, Karlsruhe, Germany. 2008.
33. N.V. Surovtsev, Suppression of spurious background in low-frequency Raman spectroscopy, Optoelectron., Instrum. Data Process. 53 (2017) 250-254.
34. B.G. Bazarov, O.D. Chimitova, R.F. Klevtsova, Y.L. Tushinova, L.A. Glinskaya, Z.G. Bazarova, Crystal structure of a new ternary molybdate in the Rb_2MoO_4-$Eu_2(MoO_4)_3$-$Hf(MoO_4)_2$ system, J. Struct. Chem. 49 (1) (2008) 53-57.
35. V.G. Grossman, B.G. Bazarov, Zh.G. Bazarova, Subsolidus phase diagrams for the Tl_2MoO_4-$Ln_2(MoO_4)_3$-$Hf(MoO_4)_2$ systems, where Ln = La-Lu, Russ. J. Inorg. Chem. 53 (11) (2008) 1788-1794.
36. V.V. Atuchin, A.K. Subanakov, A.S. Aleksandrovsky, B.G. Bazarov, J.G. Bazarova, T.A. Gavrilova, A.S. Krylov, M.S. Molokeev, A.S. Oreshonkov, S.Yu. Stefanovich, Structural and spectroscopic properties of new noncentrosymmetric self-activated borate $Rb_3EuB_6O_{12}$ with B_5O_{10} units, Mater. Des. 140 (2018) 488-494.

37. I.B. Troitskaia, T.A. Gavrilova, S.A. Gromilov, D.V. Sheglov, V.V. Atuchin, R.S. Vemuri, C.V. Ramana, Growth and structural properties of α-MoO_3 (010) microplates with atomically flat surface, Mater. Sci. Eng. B 174 (2010) 159-163.
38. V.V. Atuchin, T.A. Gavrilova, T.I. Grigorieva, N.V. Kuratieva, K.A. Okotrub, N.V. Pervukhina, N.V. Surovtsev, Sublimation growth and vibrational microspectrometry of α-MoO_3 single crystals, J. Cryst. Growth 318 (2011) 987-990.
39. V.A. Blatov, A.P. Shevchenko, D.M. Proserpio, Applied topological analysis of crystal structures with the program package ToposPro, Cryst. Growth Des., 14 (2014) 3576-3586.
40. V.G. Grossman, B.G. Bazarov, Ts.T. Bazarova, L. A. Glinskaya, J.G. Bazarova, J. Temuujin, Phase equilibria in the Tl_2MoO_4-$Ho_2(MoO_4)_3$-$Zr(MoO_4)_2$ system and the crystal structure of $Ho_2Zr_2(MoO_4)_7$ and $TlHoZr_{0.5}(MoO_4)_3$, J. Ceram. Process. Research 18 (12) (2017) 875-881.
41. K. Nakamoto, Infrared and Raman Spectra of Inorganic and Coordination Compounds. 6th ed. Wiley, New York etc., 2009.
42. P.A. Loiko, E.V. Vilejshikova, X. Mateos, J.M. Serres, V.I. Dashkevich, V.A. Orlovich, A.S. Yasukevich, N.V. Kuleshov, K.V. Yumashev, S.V. Grigoriev, S.M. Vatnik, S.N. Bagaev, A.A. Pavlyuk, Spectroscopy of tetragonal Eu:$NaGd(WO_4)_2$ crystal, Opt. Mater. 57 (2016) 1-7.

Table 1. Main parameters of processing and refinement of the $RbEu(MoO_4)_2$ sample

Compound	$RbEu(MoO_4)_2$
Sp.Gr.	*Pbcn*
a, Å	5.13502 (5)
b, Å	18.8581 (2)
c, Å	8.12849 (7)
V, Å^3	787.13 (1)
Z	4
2θ-interval, º	5-140
No. of reflections	753
No. of refined parameters	51
R_{wp}, %	1.85
R_p, %	1.86
R_{exp}, %	1.14
χ^2	1.63
R_B, %	0.86

Table 2. Correlation diagram of internal vibrations of the MoO_4^{2-} molecular group in the $RbEu(MoO_4)_2$ (Infrared active modes not included).

Free ion sym.	Site sym.	Crystal sym.
T_d	C_1	D_{2h}
A_1 (ν_1)	A	$A_g+B_{1g}+B_{2g}+B_{3g}$
E (ν_2)	$2A$	$2A_g+2B_{1g}+2B_{2g}+2B_{3g}$
T_2 (ν_3)	$3A$	$3A_g+3B_{1g}+3B_{2g}+3B_{3g}$
T_2 (ν_4)	$3A$	$3A_g+3B_{1g}+3B_{2g}+3B_{3g}$

Captions

Fig. 1. SEM pattern recorded for the $RbEu(MoO_4)_2$ particles.

Fig. 2. Measured (red), calculated (black) and differential (blue) diffraction patterns of (a) $RbEu(MoO_4)_2$.

Fig. 3.. Crystal structure of $RbEu(MoO_4)_2$. The unit cell is outlined. The lone atoms, except for Rb ones, are omitted for clarity.

Fig. 4. DSC measurements: (a) heating up to melting and (b) heating-cooling over the temperature range of 400 – 1423 K.

Fig. 5. The Raman spectra of $RbEu(MoO_4)_2$ recorded at 1064 (a) and 514.5 nm (b). The peaks related to Eu^{3+} luminescence are shown with arrows, and the artefact is shown with an asterisk.

Fig. 6. Raman spectra of Rb*Ln*$(MoO_4)_2$ molybdates (a) in the range of high-wavenumber values and (b) in the range of bending vibrations of MoO_4^{2-} ions.

Fig. 7. Photoluminescence spectrum under the excitation at 514.5 nm.

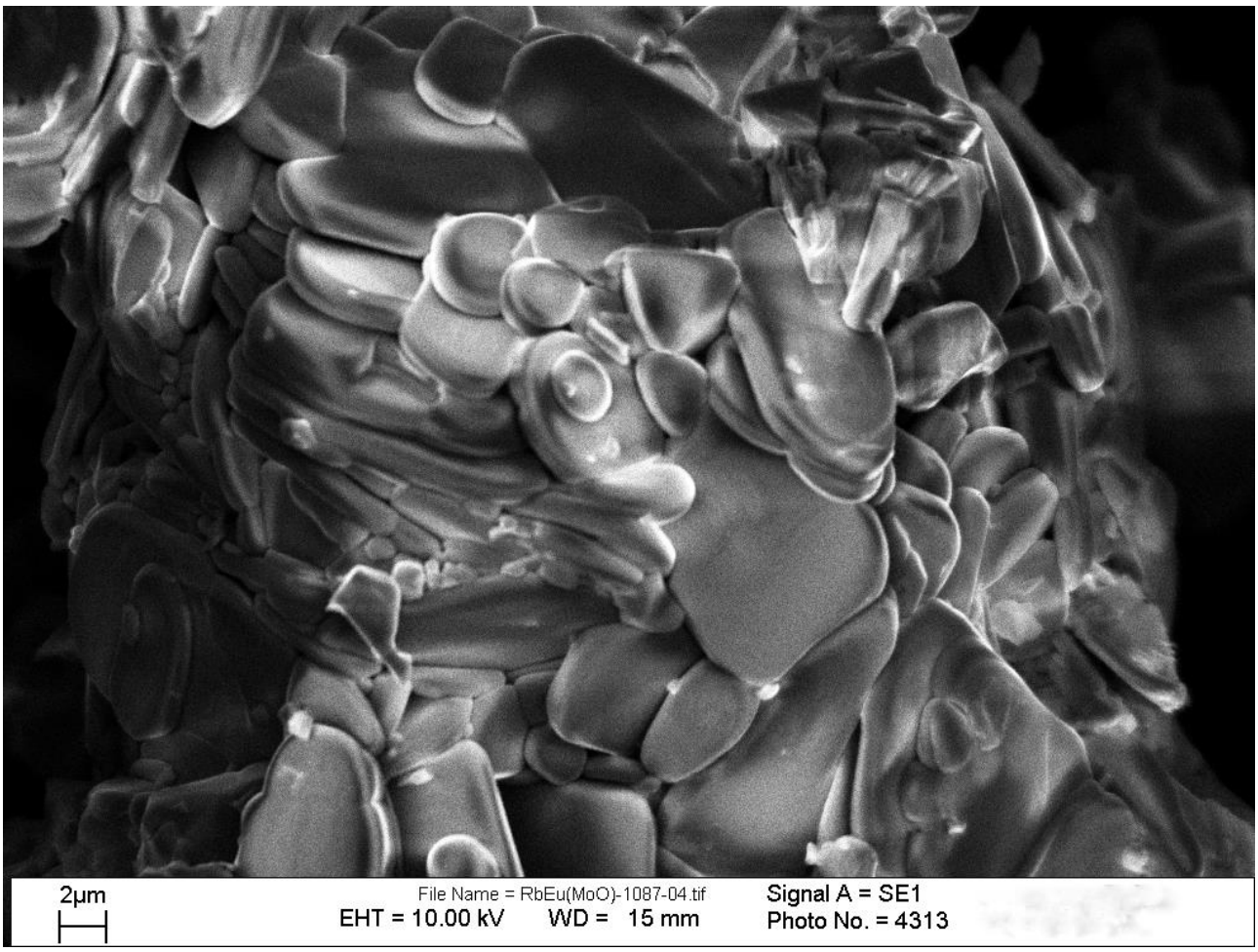
2µm
File Name = RbEu(MoO)-1087-04.tif
EHT = 10.00 kV
WD = 15 mm
Signal A = SE1
Photo No. = 4313

Fig. 1.

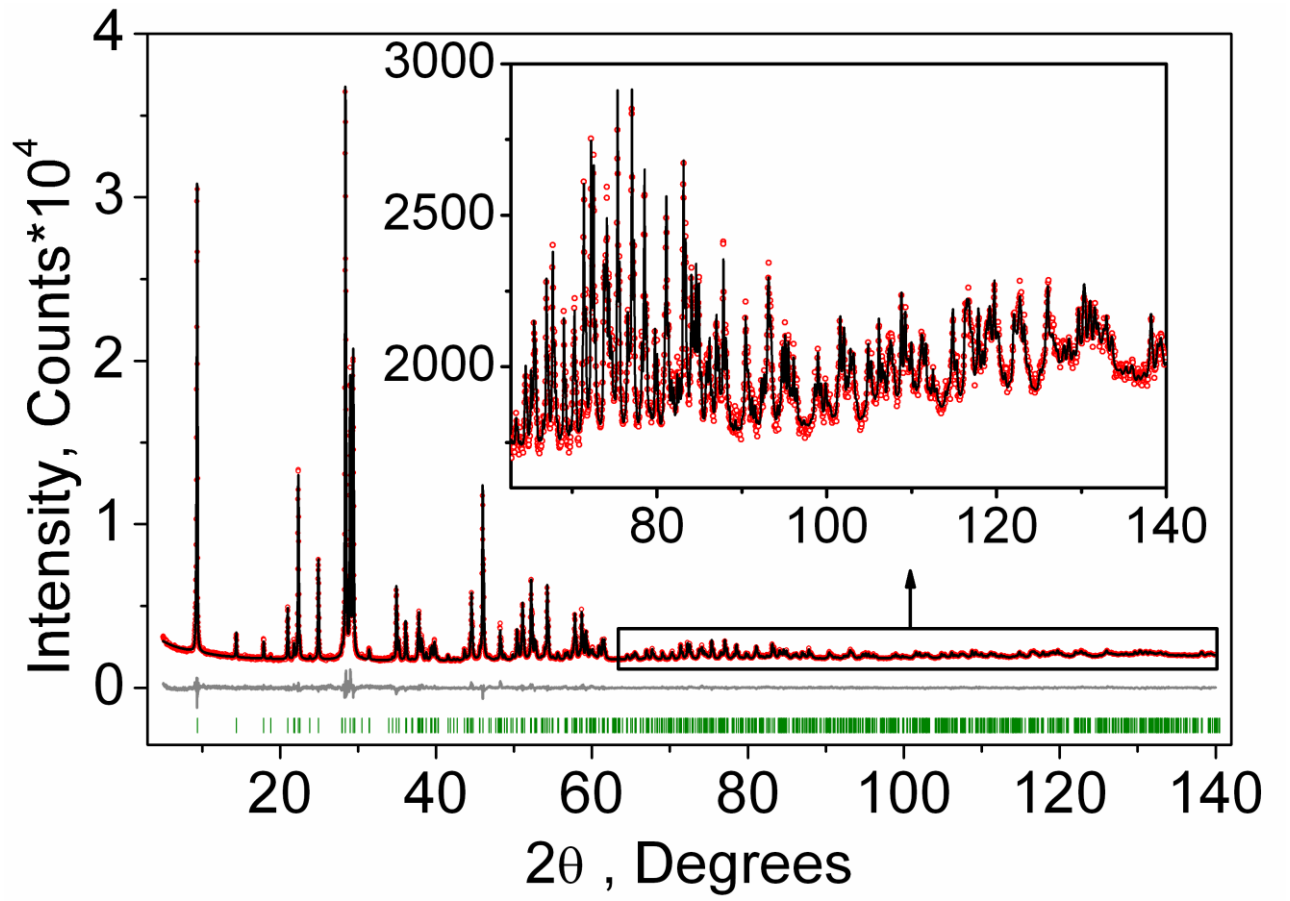
Intensity, Counts*10^4
2θ , Degrees
0
1
2
3
4
20
40
60
80
100
120
140
3000
2500
2000
80
100
120
140

Fig. 2.

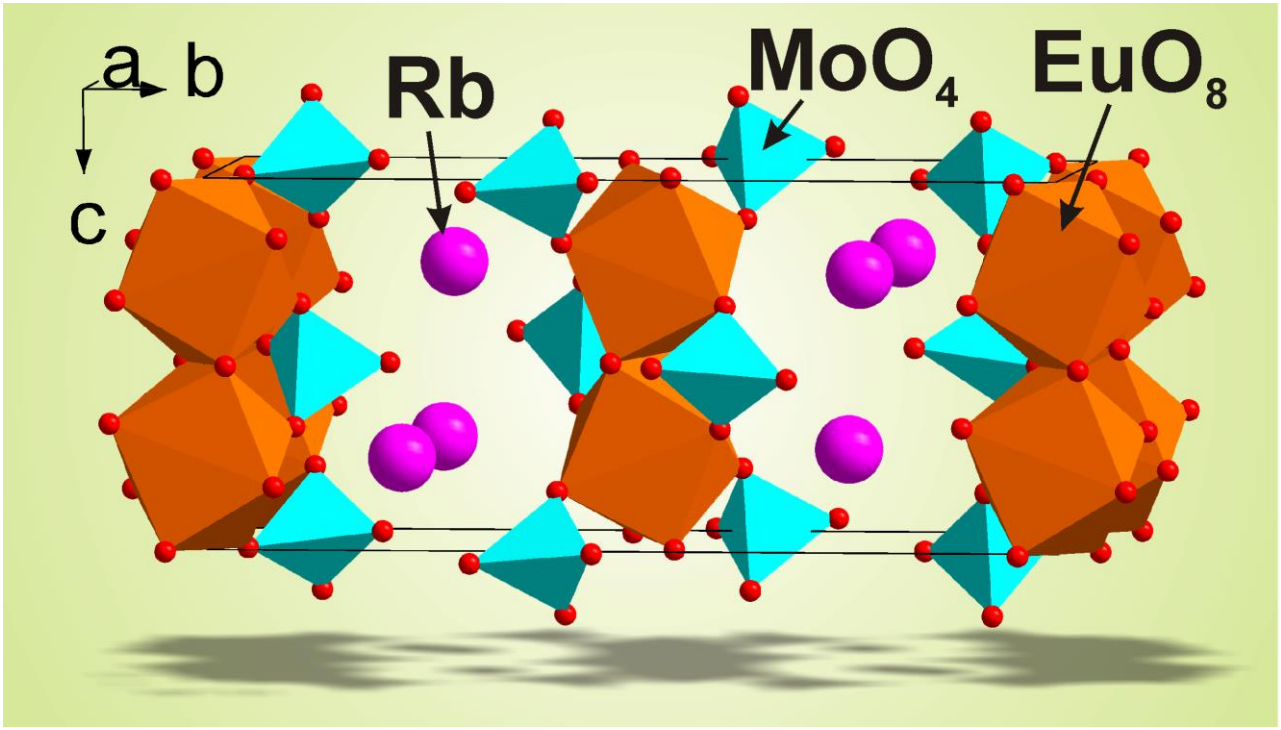

Fig. 3

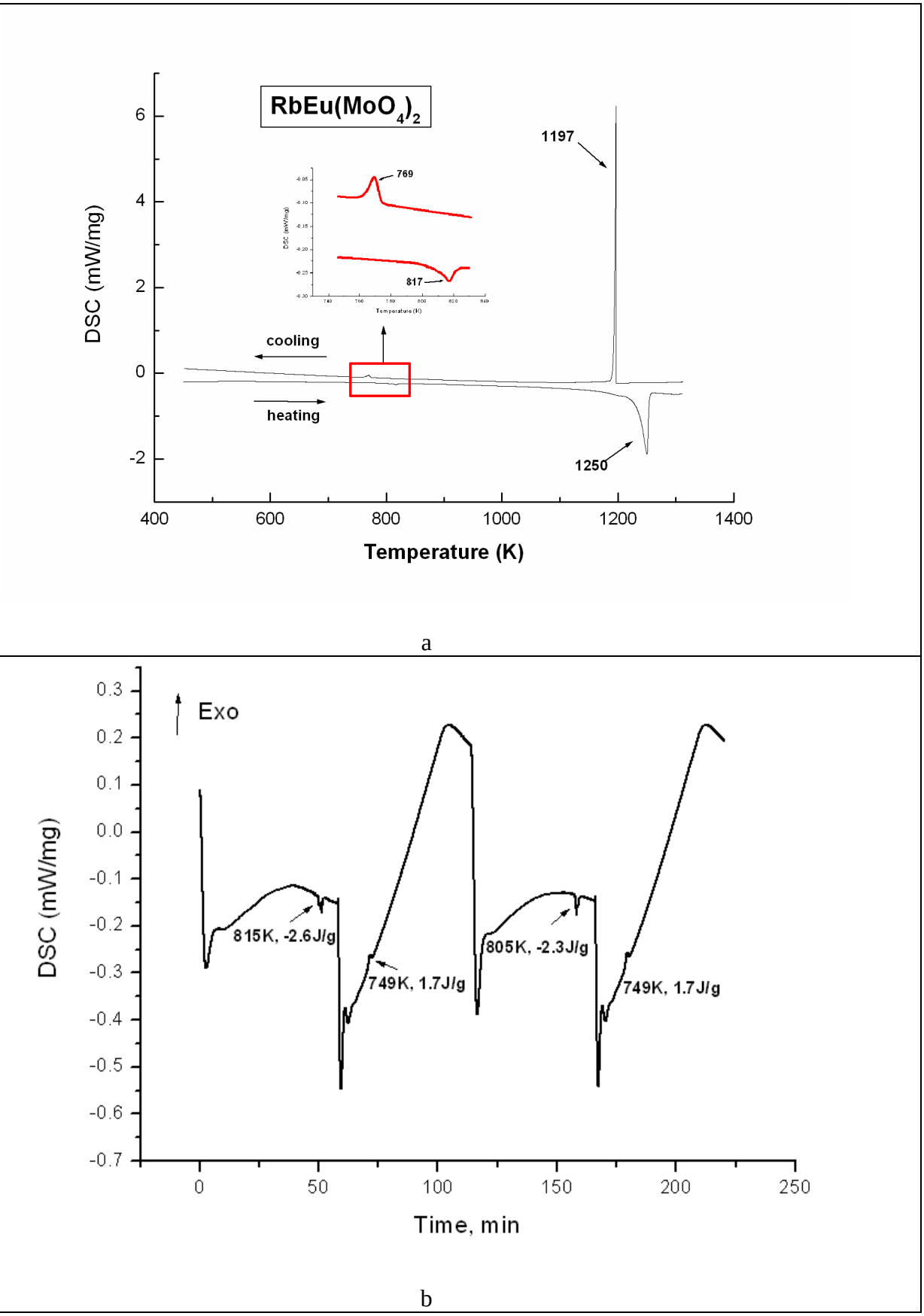
RbEu(MoO4)2
1197
769
817
cooling
heating
1250
DSC (mW/mg)
Temperature (K)
Exo
815K, -2.6J/g
749K, 1.7J/g
805K, -2.3J/g
749K, 1.7J/g
DSC (mW/mg)
Time, min

a

b

Fig. 4.

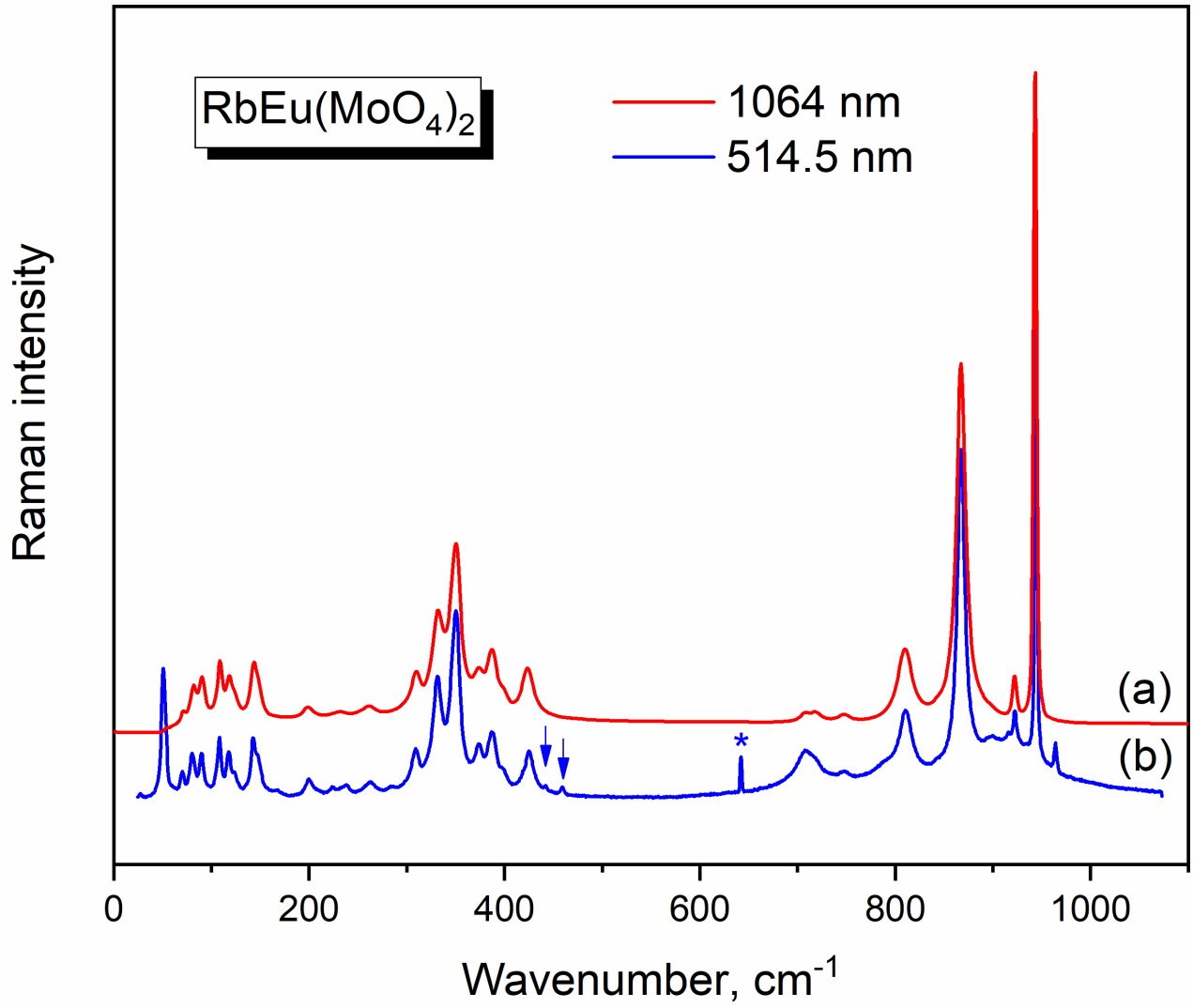
RbEu(MoO4)2
1064 nm
514.5 nm
Raman intensity
(a)
(b)
*
0
200
400
600
800
1000
Wavenumber, cm-1

Fig. 5

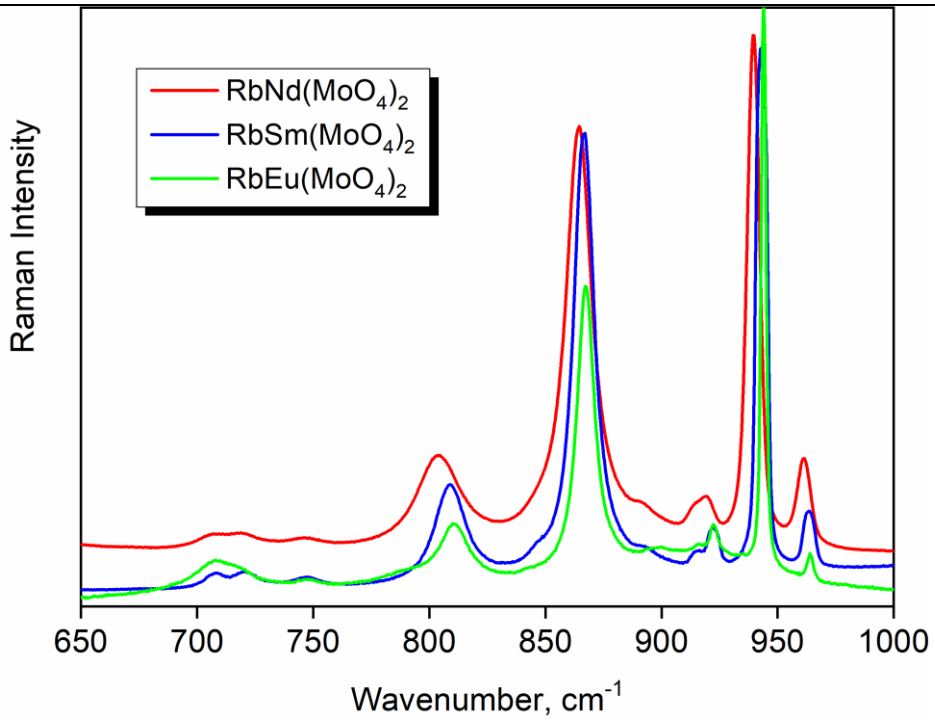
RbNd(MoO4)2
RbSm(MoO4)2
RbEu(MoO4)2
Raman Intensity
650
700
750
800
850
900
950
1000
Wavenumber, cm-1

a

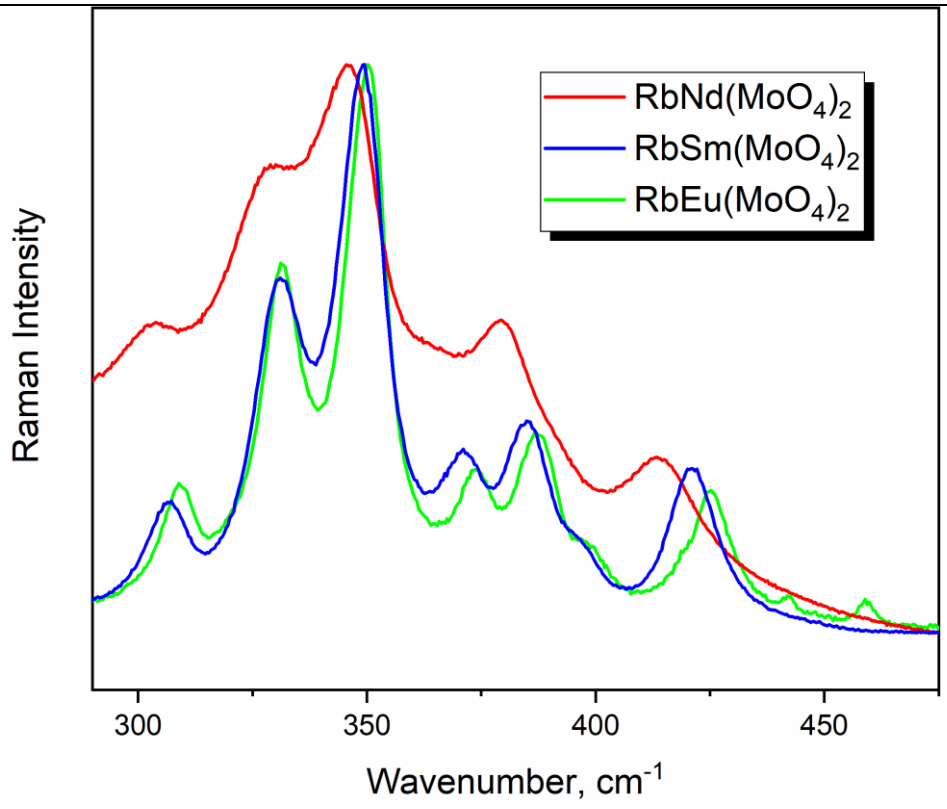
RbNd(MoO4)2
RbSm(MoO4)2
RbEu(MoO4)2
Raman Intensity
300
350
400
450
Wavenumber, cm-1

b

Fig. 6.

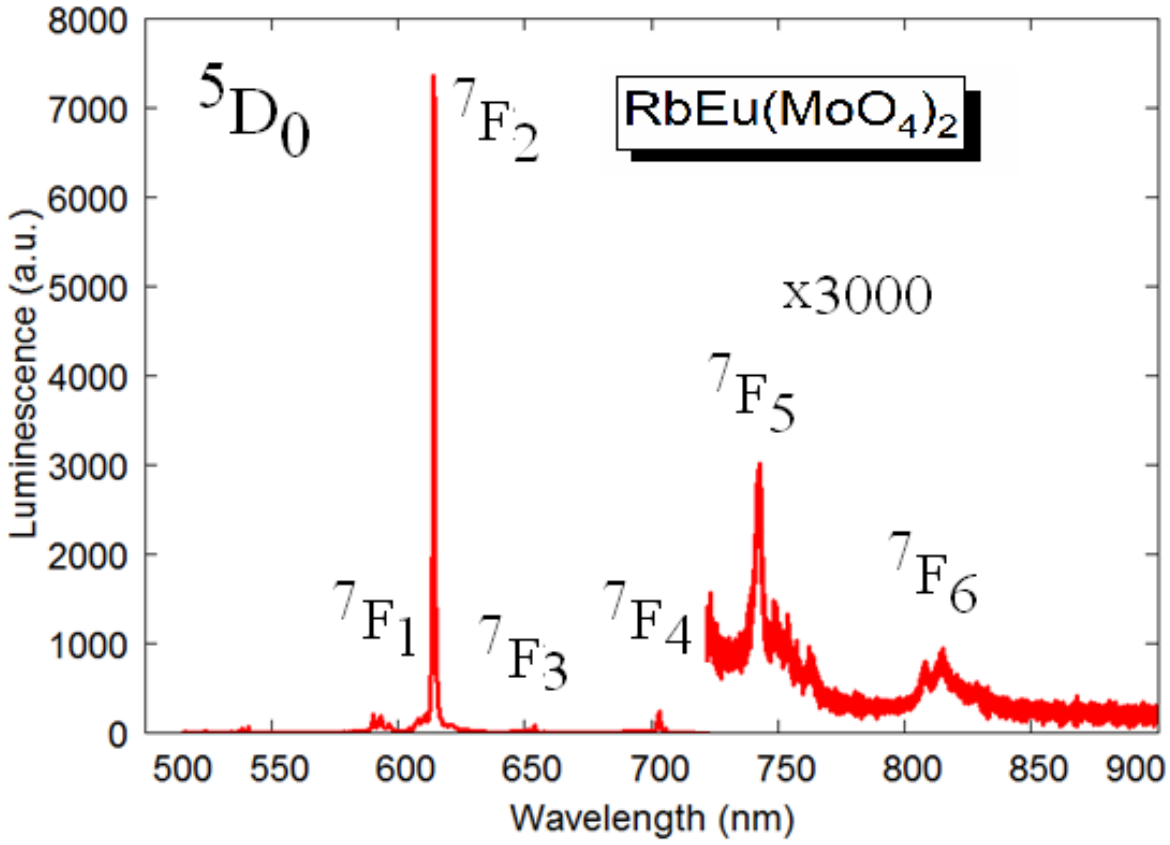
8000
7000
6000
5000
4000
3000
2000
1000
0
Luminescence (a.u.)
500
550
600
650
700
750
800
850
900
Wavelength (nm)
$^5D_0$
$^7F_2$
RbEu(MoO$_4$)$_2$
x3000
$^7F_5$
$^7F_1$
$^7F_3$
$^7F_4$
$^7F_6$

Fig. 7.